J Mater Sci (2013) 48:2416–2423
DOI 10.1007/s10853-012-7028-4

Graphene-reinforced epoxy resin with enhanced atomic oxygen erosion resistance

Wen Zhang · Min Yi · Zhigang Shen · Xiaohu Zhao · Xiaojing Zhang · Shulin Ma

Received: 26 September 2012 / Accepted: 12 November 2012 / Published online: 27 November 2012

Abstract Atomic oxygen (AO) is a dominant component of the low earth orbit and can erode most spacecraft material. We demonstrated the application of graphene to enhance AO erosion resistance of spacecraft polymers. Graphene-reinforced epoxy resin nanocomposites were prepared by solidification of epoxy resin in solution with dispersed graphene flakes and their AO erosion resistance was investigated in a plasma-type ground-based AO effects simulation facility. The nanocomposites were characterized by X-ray diffraction, scanning electron microscopy, thermogravimetric analysis, and X-ray photoelectron spectroscopy. Results based on erosion kinetics revealed that a 46 % decrease in mass loss and a 47 % decrease in erosion yield were achieved by addition of only 0.5 wt% of graphene. Further analysis of the surface morphology and composition showed that the graphene nanoflakes could serve as barriers to protect underneath from AO erosion. Thus, this approach provides a novel route for improving durability and reliability of spacecraft material, especially polymers.

W. Zhang · M. Yi · Z. Shen · X. Zhao · X. Zhang · S. Ma
Beijing Key Laboratory for Powder Technology Research and Development, Beijing University of Aeronautics and Astronautics, 37 Xueyuan Street, Beijing 100191, People's Republic of China

W. Zhang · M. Yi · Z. Shen (✉) · X. Zhao
Plasma Laboratory, Ministry-of-Education Key Laboratory of Fluid Mechanics, Beijing University of Aeronautics and Astronautics, 37 Xueyuan Street, Beijing 100191, People's Republic of China
e-mail: shenzhgbhu@gmail.com

Introduction

Graphene, a monolayer of sp^2-hybridized carbon atoms arranged in a two-dimensional lattice, has attracted increasing attention in recent years owing to its exceptional properties such as super-mechanical, electrical, thermal, and chemically inert properties [1–3]. Very recently, polymer/graphene nanocomposites have attracted a tremendous amount of attention because graphene fillers with very low loading have the potential to match or exceed the performance of large quantities of traditional composite fillers [4, 5]. However, most work within this aspect was mainly emphasized on enhancing mechanical or electrical properties of polymers by adding graphene fillers. And, exploiting the application of graphene in polymers with special functionality is still under way.

On one hand, it has been experimentally demonstrated that a monolayer graphene membrane is impermeable to standard gases [6]. Meanwhile, molecular simulations shown that even defective graphene is a suitable candidate for making impermeable nanomembranes for future applications [7]. These results indicate functional applications of graphene as light and effective materials for resisting gas penetration. Most importantly, simulation work showed that though graphene can be easily oxidized by atomic oxygen (AO) which forms strong chemical bonds on its surface, the minimum energy barrier for an oxygen atom passing from the top to the bottom side of monolayer graphene is as high as 5.98 eV and graphene with more layers will pose higher energy barrier [8]. Accordingly, it can be anticipated that graphene flakes could protect the polymer underneath from AO erosion because they pose a high energy barrier to AO diffusing from the top of the graphene flakes to the reactive polymer surface underneath.

On the other hand, it has been well known that AO, the dominant component and the most active species of the low earth orbit (LEO) atmosphere, can result in erosion and degradation of most spacecraft material [9, 10]. The translational energy of AO collisions is about 4.5–5 eV, which is sufficient to break the polymer bond and induce oxidative decomposition [11, 12]. Epoxy resin is a thermosetting polymer widely used on spacecraft. It has excellent mechanical and chemical properties, including high dimension stability, hardness, flexibility, and excellent chemical resistance [13]. However, epoxy resin is susceptible for the AO attack and cannot meet the requirements of long lifetime spacecrafts [14]. Hence, much work has been carried out to obtain an AO erosion-resistant epoxy resin. So far, several methods have been conducted to protect material from erosion, one of which is to disperse fillers into the matrix. Such fillers can resist AO erosion and in the micron- or nanosized range. Moreover, filling particles can make composites still possess high AO erosion resistance even when large and deep defects appear on the material surface [15].

Taking these above-mentioned considerations into account, here we turn to the application of graphene in spacecraft material and investigate the AO erosion resistance of graphene-reinforced epoxy resin. In this paper, nanocomposites were prepared by incorporating graphene flakes into an epoxy resin matrix using acetone as the processing solvent followed by a solidification process [16]. The graphene flakes prepared here by jet cavitation method were characterized by atomic force microscopy (AFM), transmission electron microscopy (TEM), and Raman spectrum and X-ray diffraction (XRD). The nanocomposites were characterized by XRD, scanning electron microscopy (SEM), thermogravimetric analysis, and X-ray photoelectron spectroscopy (XPS). AO erosion resistance of these nanocomposites with different graphene loadings was investigated by exposure experiments in a plasma-type ground-based AO effects simulation facility. The effect of graphene flakes on the AO erosion resistance of epoxy resin was analyzed and the AO erosion resistant mechanism was discussed.

Experimental

Preparation of graphene

Graphene dispersion was prepared by a jet cavitation method which was reported previously [17]. First, graphite dispersion with an initial graphite concentration of 3 mg mL^{-1} was first treated in the designed jet cavitation device under pressure 20 MPa for 1 h. Second, the treated dispersion was centrifuged by a centrifuge (L-600, Changsha XiangYi, China) at 2000 rpm (×568*g*) for 30 min to remove large particles. Then, the supernate was collected as graphene dispersion for further characterization and application. Finally, a large quantity of the above supernatant was vacuum filtered through a nylon membranes (pore size 450 nm) supported on a fritted glass holder [18]. The obtained filter cakes were peeled out of the membranes and further dried overnight in a vacuum oven at 80 °C. The dried graphene cakes were retained for use in preparing nanocomposites.

Preparation of epoxy resin/graphene nanocomposites

First, dried graphene cakes of specified mass were redispersed in acetone in a sonic bath (KX-1620HG, Beijing Kexi, China). Second, the epoxy resin (E51, a class of bisphenol A epoxy resin) with calculated mass was introduced into the above suspension followed by further bath sonication for 30 min at room temperature to achieve uniform dispersion. This method is more efficient at dispersing fillers into viscous systems compared with other techniques, such as conventional stirring [19]. Third, solvents and gas were removed in a vacuum oven for 2 h at 70 °C [20, 21]. Subsequently, a stoichiometric amount of curing agent, ethidene diamine, was added to the above graphene/epoxy resin mixtures followed by degassing in a vacuum oven for 3 h to remove gas [22]. In the final step, the mixtures were cast onto a glass plate and cured at room temperature for 5 h, 50 °C for 5 h, and 80 °C for 5 h.

We prepared epoxy resin/graphene nanocomposites by the solution mixing method and performed AO effects simulation experiments. Our motivation was to examine if the addition of graphene can improve the AO erosion resistance of material. To study the effect of different graphene loadings on the AO resistance, nanocomposites with 0, 0.05, 0.1, and 0.5 wt% graphene loadings were prepared.

Atomic oxygen effects simulation experiment

The AO exposure experiment of all samples was conducted in the ground-based AO effects simulation facility designed by our group, in which AO is generated by discharging the cathode filament confined by a multiple magnetic field [23]. During the experiment, samples were placed on a circular holder in the vacuum chamber of the facility, in which the pressure was 0.15 Pa. In order to know the mass change of samples during the AO exposure, samples were periodically removed from the vacuum chamber and weighed. The mass loss of Kapton could be used as a standard to calculate the AO fluence by the following equation [24]:

$$F = \frac{\Delta M_{\mathrm{k}}}{\rho A E_{\mathrm{y}}} \quad (1)$$

Here, F is the AO fluence (atom cm^{-2}), ΔM_{k} is the mass loss of the Kapton sample (g), ρ is the density of Kapton

(g cm^{-3}), A is the area of the Kapton sample (cm^2), and E_y is the erosion yield of Kapton (in general $E_y = 3.0 \times 10^{-24}$ cm^3 $atom^{-1}$). In this study, for a test period of about 50 h, the AO fluence was about 11.8×10^{20} atoms/cm^2, which was equivalent approximately to the AO fluence of 253 days at an altitude of 400 km.

Characterization

Height profile and morphology of graphene flakes were investigated with AFM CSPM5500 (Being Nano-Instruments, China) equipped with a 13.56-m scanner in tapping mode. TEM imaging of graphene flakes and nanocomposites was performed using a JEOL JEM-2010FEF operated at 200 kV. Raman spectrum was collected on a dried graphene cake. The Raman measurements were made on these filtered and dried graphene cakes using a Renishaw Rm2000 using a 514-nm laser. XRD patterns of these nanocomposites and graphene cake were gained using a Bruke D8 Advance. The mass of samples before and after AO exposure was measured using a DT-100 balance with a sensitivity of 0.00005 g. Surface morphology of samples was measured using a LEO 1530VP SEM. Surface compositions of the samples were determined using an ESCALAB-250 X-ray photoelectron spectrometer (XPS).

Results and discussion

Characterization of graphene and epoxy resin/graphene nanocomposites

Knowledge about the lateral size of the graphene here prepared by jet cavitation method is important for preparing epoxy resin/graphene nanocomposites. AFM and TEM were utilized to visually gain the information about lateral size. A representative AFM image in Fig. 1a shows the deposited individual graphene flake with lateral size of ~1.6 μm and thickness of ~0.77 nm, which may be monolayer or at most bilayer. Figure 1b illustrates a typical bright field TEM of several graphene flakes deposited on a TEM grid. The flake lateral size is around several micrometers with some large flakes of ~5 μm. It should be noted that the large flakes play an important role in enhancing mechanical interlocking and inhibiting gas diffusion in the nanocomposites. The graphene used for reinforcing epoxy is composed of such individual graphene flakes. These individual graphene flakes can be made into cakes by vacuum filtering the graphene dispersion through porous membrane. The Raman spectrum and XRD spectrum of the graphene cake is presented in Figs. 1c and 2b, respectively. The 2D band of the graphene cake is obviously different from that of the pristine graphite, indicating the nature of few-layer graphene [25]. The graphene cake is made of thin and small graphene flakes, the crystalline size of which is much smaller than that of pristine graphite. As a consequence, as shown in Fig. 2a, b, for the graphene cake, the intensity of the (0002) peak sharply decreases, the (0004) and $(10\bar{1}1)$ peaks disappear, and the FWHM of the (0002) peak increases as a result of Scherrer broadening [26, 27].

X-ray diffraction is also an important tool for determining whether fillers are present individually in nanocomposites. Fig. 2 shows the XRD patterns of graphite, graphene cake, pure epoxy resin, and epoxy resin/graphene nanocomposites with varying contents. The typical diffraction peak of graphene was observed at around 26.6° and a very broad peak at around 20° of the pure epoxy resin was observed due to its amorphous nature. The XRD patterns of nanocomposites only showed the diffraction peak of the pure epoxy resin, whereas the crystalline peak of

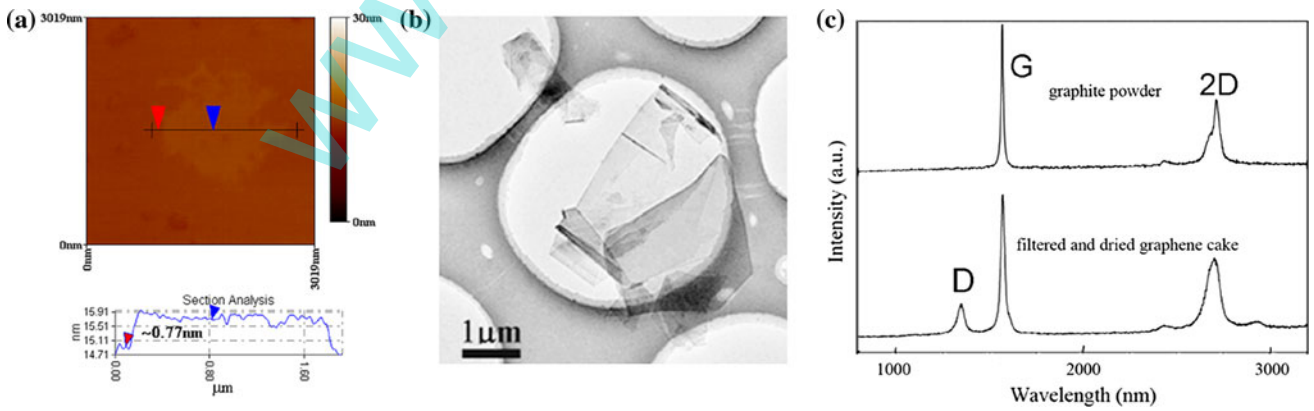

Fig. 1 **a** A representative AFM image of a monolayer graphene. **b** A typical bright field TEM of several few-layer graphene flakes. **c** Raman spectra measured at 514 nm excitation for a dried graphene cake fabricated by vacuum filtration and pristine graphite powder. The intensity was normalized by G peak

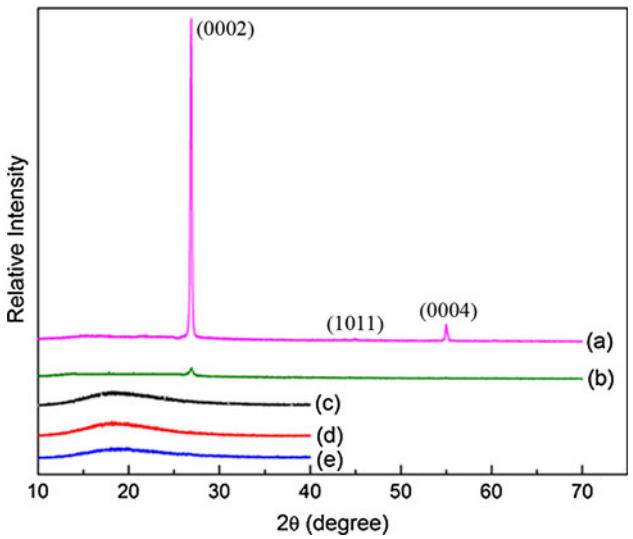

Fig. 2 XRD patterns of **a** pristine graphite powder, **b** dried graphene cakes **c** pure epoxy resin, **d** epoxy resin/graphene nanocomposites with graphene loading of 0.1 wt%, and **e** 0.5 wt%

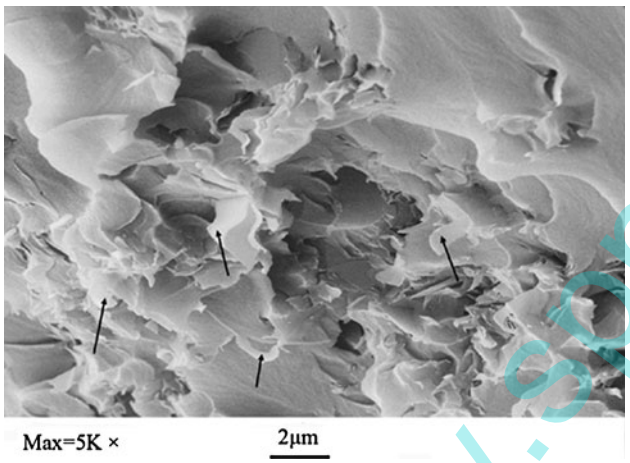

Fig. 3 A SEM image of a fracture surface of nanocomposite with a graphene loading of 0.5 wt%

graphene disappeared, indicating that graphene was fully dispersed into individual nanoflakes in the resin matrix and the regular and periodic structure of graphene disappeared [28, 29].

Figure 3 shows a SEM image of the fractured surface of an epoxy resin/graphene nanocomposite sample with 0.5 wt% graphene, in which black arrows point to graphene flakes. It can be seen clearly that graphene flakes protrude out of the fracture surface and several thin and transparent graphene flakes are clearly well-dispersed in the epoxy resin matrix. Figure 4 and Table 1 compare the thermal stability of the pure epoxy resin and the nanocomposite containing 0.5 wt% graphene. There are two steps in the degradation of the nanocomposite [30]: The first step, from

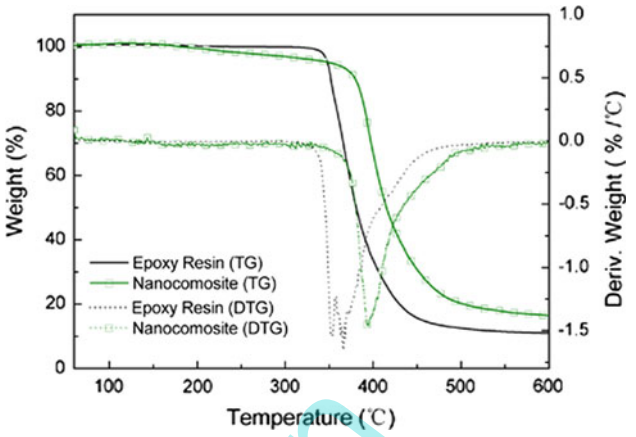

Fig. 4 TG and DTG curves of epoxy resin and nanocomposite containing 0.5 wt% graphene nanoflakes (heating rate 20 °C min^{-1}, N_2 flow 30 mL min^{-1})

Table 1 Comparison of TG results between the pure epoxy resin and the nanocomposite containing 0.5 wt% graphene nanoflakes

Material	Half life temperature (°C)	Final degradation temperature (°C)	Char residue contents (%)
Epoxy resin	381.0	536.2	11.0
Nanocomposite	415.3	579.6	16.4

around 200 °C, is due to the existence of water and other solvent in the graphene; the second step, roughly from 400 °C, which is the degradation of the polymer, has shifted to a higher temperature range than for the pure epoxy resin. This suggests strong interaction between the resin matrix and graphene at the interface, which would decrease the mobility of polymer chains and increase the thermal stability of nanocomposites. Moreover, the nanocomposite have a char residue higher than the graphene content, which is attributed to the presence of charred graphene flakes inhibiting further thermal degradation of resin molecules [31]. Obviously, the improvement of the thermal stability also contributes to the durability of epoxy resin/graphene nanocomposites in the space environment, where the variation of temperature is tremendous.

Atomic oxygen resistance of epoxy resin/graphene nanocomposites

Figure 5 is the mass loss and the erosion yield (volume of material removed per oxygen atom arriving) versus AO fluence for different samples [32]. At the beginning of the exposure experiment, the mass loss of these samples is nearly the same because surfaces of nanocomposites are

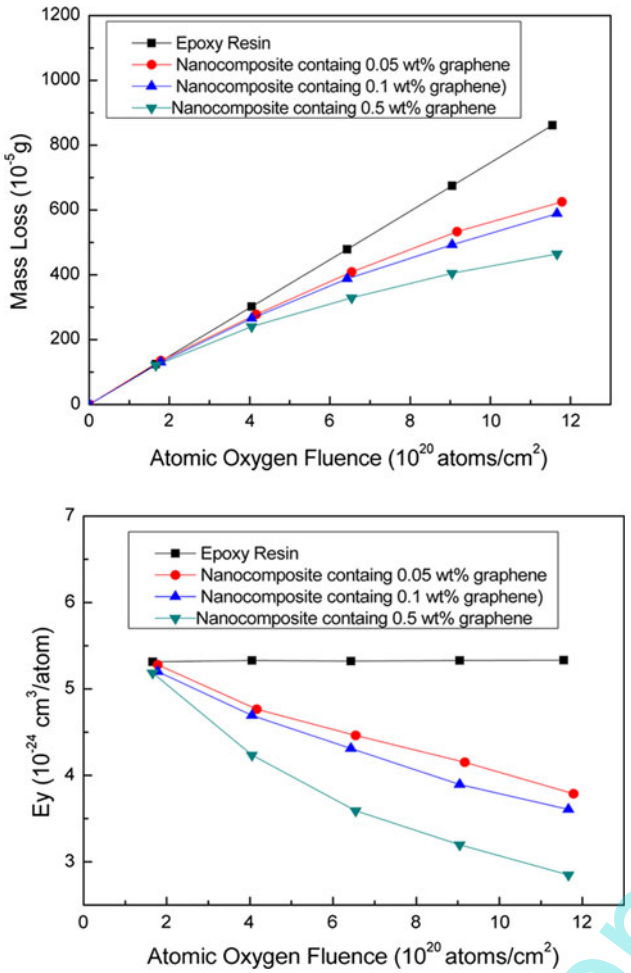

Fig. 5 Mass loss and erosion yield of the epoxy resin and nanocomposites

almost composited of resin and the graphene was covered. However, the mass loss of the pure epoxy resin increases linearly with the AO fluence; in other words, the erosion yield is a fixed value. In contrast, as the AO fluence increases, the mass of nanocomposites loses at an increasing slow rate, namely the erosion yield reduces, which indicates that the AO erosion resistance is improved by filling graphene flakes. Furthermore, the larger the filling amount of graphene, the better the AO erosion resistance of nanocomposites. After 50-h exposure, the mass loss and the erosion yield of the nanocompoiste containing 0.5 wt% graphene decrease to 54 and 53 % of those of the pure epoxy resin, respectively.

Figure 6 shows the surface morphology of the pure epoxy resin sample before and after AO exposure. The surface of the pure epoxy resin sample is smooth and uniform before AO exposure. After the AO exposure experiment, the surface is significantly roughened and forms the "corduroy-like" structures, indicating that the epoxy resin is eroded significantly by AO. Figure 7 shows surface morphology of the nanocomposite containing 0.5 wt% graphene before and after AO exposure. Comparing Figs. 6 and 7, it can be seen that the surface characteristic of the nanocomposite sample is significantly different from that of the epoxy resin sample after the AO exposure. The surface of the nanocomposite is just slightly accidented, suggesting that the AO do not erode it severely and it can resist the AO erosion. In contrast, Fig. 8 shows the difference of surface morphology between the pure epoxy resin and the nanocomposite. Graphene nanoflakes are on the surface of the nanocomposite clearly as shown in Fig. 8b, in which the resin on the surface was eroded at the early stage and graphene flakes are exposed subsequently. With the increased AO fluence, more and more graphene nanoflakes are exposed and covered the underlying resin to prevent resin from further AO erosion.

Figure 9 shows XPS spectra of epoxy resin and nanocomposite samples before and after the AO exposure. Table 2 indicates the carbon content and the oxygen content of epoxy resin have little change because the interaction between epoxy resin and AO forms volatile oxidation products. In contrast, the carbon content of the nanocomposite decreases significantly, while the oxygen content increases. It indicates that graphene nanoflakes remain on the material surface after oxidation, which is in agreement with the analysis of surface morphology.

The AO erosion resistance of epoxy resin/graphene nanocomposites contributes to the following factors: AO erosion begins with AO diffusing into material. It is reported that gas permeability through polymer films can be reduced by 50–500 times even with small loadings of nanoflakes. The dispersion of impenetrable graphene of the high aspect ratio and surface area into polymer matrices provides a tortuous path for the diffusing gas atoms, enhancing the gas barrier properties as compared to neat polymer [33–35]. The barrier properties of the nanocomposites may further be improved by the addition of fillers which can react with the penetrating gas and stop the gas from advancing their diffusion. Graphene can easily be oxidized by AO which forms strong chemical bonds. With more and more graphene exposing on the surface, it can protect the underneath from erosion by posing a high-energy barrier to any absorbed oxygen atom diffusing from the top of the graphene to the interface between the graphene and the reactive surface underneath [36]. In addition, graphene is oxidized and epoxy groups form on the surface of graphene after the AO experiment [8]. Basic thermodynamic considerations show that it would take more than 6 eV to decompose the epoxy group to molecular CO [37], which is higher than the energy of AO collisions.

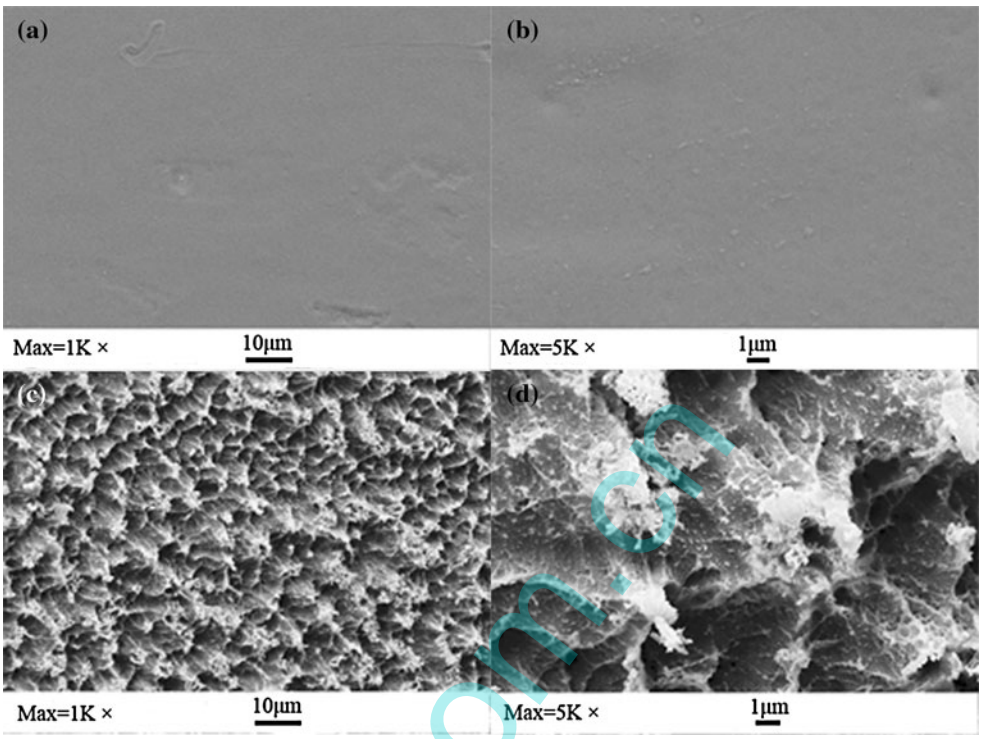

Fig. 6 SEM photographs of the epoxy resin **a**, **b** before the AO exposure and **c**, **d** after the AO exposure

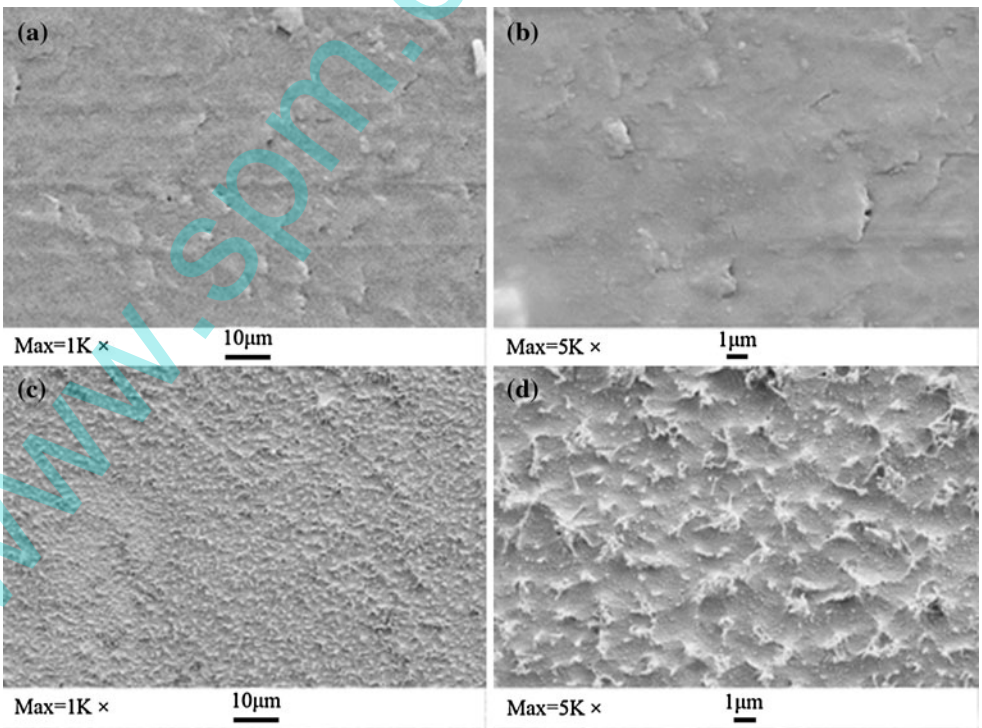

Fig. 7 SEM photographs of the nanocomposite containing 0.5 wt% graphene nanoflakes **a**, **b** before the AO exposure, **c**, **d** after the AO exposure

Conclusions

In this study, epoxy resin/graphene nanocomposites were prepared by the solution mixing method. The results of XRD and SEM analyses show the graphene homogeneously distributed in the matrix and the TGA result indicates that the thermal stability of the nanocomposite is improved. Compared with the pure epoxy resin,

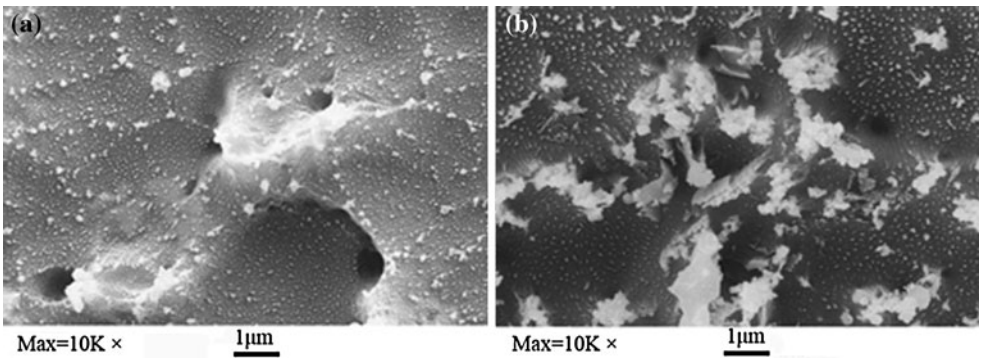

Fig. 8 SEM photographs after the AO exposure of **a** the pure epoxy resin, **b** the nanocomposite containing 0.5 wt% graphene nanoflakes

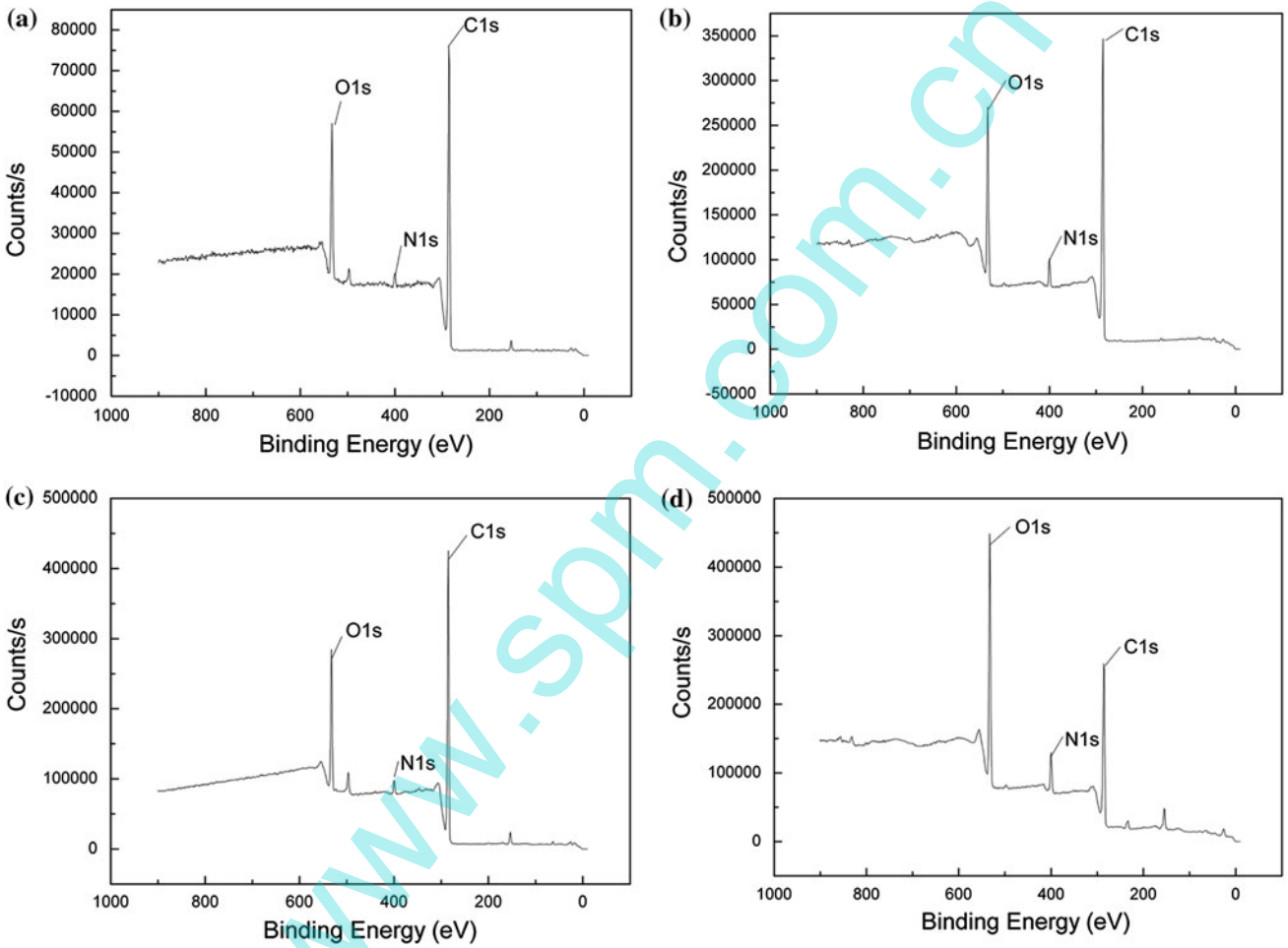

Fig. 9 XPS spectrums of **a**, **b** the epoxy resin before and after the AO experiment, **c**, **d** the nanocomposite containing 0.5 wt% graphene nanoflakes before and after the AO experiment

Table 2 Surface composition of the pure epoxy resin and the nanocomposite containing 0.5 wt% graphene nanoflakes before and after exposure to AO

Material	Treatment	Surface content by XPS (%)		
		C	O	N
Epoxy resin	Before the AO experiment	82.419	15.160	2.421
	After the AO experiment	77.279	18.231	4.49
Nanocomposite	Before the AO experiment	82.313	15.132	2.555
	After the AO experiment	58.462	33.243	8.295

the AO erosion resistance of epoxy resin/graphene nanocomposites is improved. A 46 % decrease in mass loss and a 47 % decrease in erosion yield were achieved by the addition of only 0.5 wt% of graphene. And, SEM and XPS analyses present evidence that after the resin on the nanocomposites surface is eroded, the graphene flakes are exposed on the surface and protect the material underneath from AO erosion. The AO erosion resistance is also ascribed to a tortuous path for the diffusing gas atoms because of the graphene flakes dispersed in epoxy resin and the high-energy bond formed by the interaction between graphene and AO. In principle, this method can be applied to enhance AO erosion resistance of spacecraft material and extend the life time of spacecrafts.

Acknowledgements This work was supported by the Special Funds for Co-construction Project of Beijing Municipal Commission of Education, the "985" Project of Ministry of Education of China, and the Fundamental Research Funds for the Central Universities.

References

1. Song P, Cao Z, Cai Y, Zhao L, Fang Z, Fu S (2011) Polymer 52:4001
2. Woo RC, Chen Y, Zhu H, Li J, Kim J, Leuing CY (2007) Compos Sci Technol 67:3448
3. Wojtoniszak M, Zielinska B, Chen X, Kalenczuk RJ, Borowiak-Palen E (2012) J Mater Sci 47:3185. doi:10.1007/s10853-011-6153-9
4. Li B, Zhong W (2011) J Mater Sci 46:5595. doi:10.1007/s10853-011-5572-y
5. Jang BZ, Zhamu A (2008) J Mater Sci 43:5092. doi:10.1007/s10853-008-2755-2
6. Bunch JS, Verbridge SS, Alden JS, Zande AM, Parpia JM, Craighead HG, McEuen PL (2008) Nano Lett 8(8):2458
7. Leenaerts O, Partoens B, Peeters FM (2008) Appl Phys Lett 93:193107
8. Vinogradov NA, Schulte K, Ng ML (2011) J Phys Chem 115:9568
9. Shimamura H, Nakamura T (2009) Polym Degrad Stab 94:1389
10. Devapal D, Packirisamy S, Reghunadhan CP, Ninan KN (2006) J Mater Sci 41:5764. doi:10.1007/s10853-006-0109-5
11. Su L, Tao L, Wang T, Wang Q (2012) Polym Degrad Stab 97:981
12. Xiao F, Wang K, Zhan M (2012) J Mater Sci 47:4904. doi:10.1007/s10853-012-6363-9
13. Jana S, Zhong WH (2009) J Mater Sci 44:1987. doi:10.1007/s10853-009-3293-2
14. Young PR, Slemp WS, Whitley KS, Kalil CR, Siochi EJ, Shen JY, Chang AC (1995) NASA 95-23899
15. Wang X, Zhao X, Wang M, Shen Z (2007) Polym Eng Sci 47:1156
16. Potts JR, Dreyer DR, Bielawski CW, Ruoff RS (2011) Polymer 52:5
17. Shen Z, Li J, Yi M, Zhang X, Ma S (2011) Nanotechnology 22:365306
18. Wajid AS, Das S, Irin F, Ahmed HT, Shelburne JL, Parviz D, Fullerton RJ, Jankowski AF, Hedden RC, Green MJ (2012) Carbon 50:526
19. Serena Saw WP, Mariatti M (2012) J Mater Sci: Mater Electron 23: 817. doi: 10.1007/s10854-011-0499-2
20. Kuilla T, Bhadra S, Yao D, Kim NH, Bose S (2010) Prog Polym Sci 35:1350
21. Cong H, Radosz M, Towler BF, Shen Y (2007) Sep Purif Technol 55:281
22. Zaman I, Phan TT, Kuan H, Meng Q, La LTB, Luong L, Youssf O, Ma J (2001) Polymer 52:1603
23. Zhao X, Shen Z, Xing Y, Ma S (2005) Polym Degrad Stab 88:275
24. Wang M, Zhao X, Shen Z, Ma S, Xing Y (2004) Polym Degrad Stab 86:521
25. Lotya M, Hernandez Y, King PJ, Smith RJ, Nicolosi V, Karlsson LS, Blighe FM, De S, Wang Z, McGovern IT, Duesberg GS, Coleman JN (2009) J Am Chem Soc 131(10):3611
26. Morant RA (1970) J Phys D Appl Phys 3:1367
27. Wilson NR, Pandey PA, Beanland R, Young RJ, Kinloch IA, Gong L, Gong L, Liu Z, Suenaga K, Rourke JP, York SJ, Sloan J (2009) ACS Nano 3:2547
28. Du X, Yu Z, Dasari A, Ma J, Mo M, Meng Y, Mai Y (2008) Chem Mater 20:2066
29. Du XS, Xiao M, Meng YZ, Hay AS (2005) Carbon 43:195
30. Liu N, Luo F, Wu H, Liu Y, Zhang C, Chen J (2008) Adv Funct Mater 18:1518
31. Kuila T, Bose S, Khanra P, Kim NH, Rhee KY (2011) Compos A 42:1856
32. Rutledge SK, Banks BA (1994) AIAA 94:2628
33. Singh V, Joung D, Zhai L, Das S, Khondaker S, Seal S (2011) Prog Mater Sci 56:1178
34. Suprakas SR, Masami O (2003) Prog Mater Sci 28:1539
35. Choudalakis G, Gotsis AD (2009) Eur Polym J 45:967
36. Topsakal M, Sahin H, Ciraci S (2012) Phys Rev B: Condens Matter 85:155445
37. Sun T, Fabris S, Baroni S (2011) J Phys Chem 115:4730